ACS APPLIED ENERGY MATERIALS

www.acsaem.org Article

Lithium–Oxygen Battery Exploiting Highly Concentrated Glyme-Based Electrolytes

Vittorio Marangon, Celia Hernandez-Rentero, Stanislav Levchenko, Giacomo Bianchini, Davide Spagnolo, Alvaro Caballero, Julian Morales,* and Jusef Hassoun*

Cite This: *ACS Appl. Energy Mater.* 2020, 3, 12263–12275 Read Online

ACCESS | Metrics & More | Article Recommendations | Supporting Information

ABSTRACT: Concentrated solutions of lithium bis-(trifluoromethanesulfonyl)imide (LiTFSI) and lithium nitrate ($LiNO_3$) salts in either diethylene-glycol dimethyl-ether (DEGDME) or triethylene-glycol dimethyl-ether (TREGDME) are herein characterized in terms of chemical and electrochemical properties in view of possible applications as the electrolyte in lithium–oxygen batteries. X-ray photoelectron spectroscopy at the lithium metal surface upon prolonged storage in lithium cells reveals the complex composition and nature of the solid electrolyte interphase (SEI) formed through the reduction of the solutions, while thermogravimetric analysis shows a stability depending on the glyme chain length. The applicability of the solutions in the lithium metal cell is investigated by means of electrochemical impedance spectroscopy (EIS), chronoamperometry, galvanostatic cycling, and voltammetry, which reveal high conductivity and lithium transference number as well as a wide electrochemical stability window of both electrolytes. However, a challenging issue ascribed to the more pronounced evaporation of the electrolyte based on DEGDME with respect to TREGDME actually limits the application of the former in the Li/O_2 battery. Hence, EIS measurements reveal a very fast increase in the impedance of cells using the DEGDME-based electrolyte upon prolonged exposure to the oxygen atmosphere, which leads to a performance decay of the corresponding Li/O_2 battery. Instead, cells using the TREGDME-based electrolyte reveal remarkable interphase stability and much more enhanced response with specific capacity ranging from 500 to 1000 mA h g^{-1} referred to the carbon mass in the positive electrode, with an associated maximum practical energy density of 450 W h kg^{-1}. These results suggest the glyme volatility as a determining factor for allowing the use of the electrolyte media in a Li/O_2 cell. Therefore, electrolytes using a glyme with sufficiently high boiling point, such as TREGDME, which is further increased by the relevant presence of salts including a lithium protecting sacrificial one ($LiNO_3$), can allow the application of the solutions in a safe and high-performance lithium–oxygen battery.

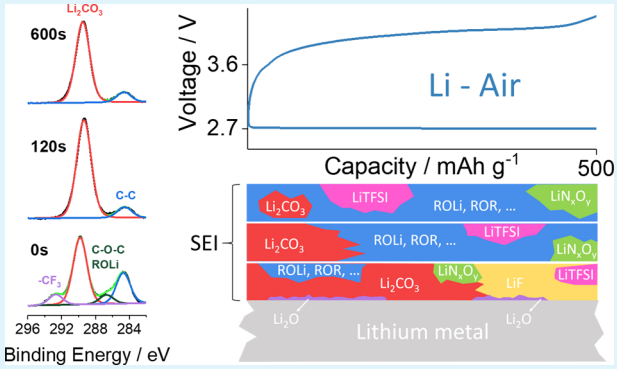

KEYWORDS: *glyme electrolyte, $LiNO_3$, LiTFSI, highly concentrated, lithium–oxygen battery*

INTRODUCTION

Increasing demand for environmentally sustainable energies has triggered the rapid development of systems employing renewable sources, promoted the electrified mobility, and concomitantly fetched the research for efficient electrochemical storage devices such as the lithium-ion batteries.[1] The Li-ion battery based on the reversible intercalation of Li^+ ions into the electrode structure has achieved a relevant energy density, that is, exceeding 250 W h kg^{-1}, and an extended cycle life.[2,3] However, the rapid evolution of the electric vehicle market recently posed challenging issues on the expected relevant economic impact and the relatively limited driving range ascribed to the Li-ion battery.[4,5] A lithium metal electrode is characterized by the notable theoretical capacity of 3860 mA h g^{-1} and by the lowest redox potential, that is, −3.04 V *versus* SHE,[6,7] while oxygen is the most abundant and light oxidant in the earth atmosphere. Therefore, an emerging system such as a lithium–oxygen (Li/O_2) battery so far appeared as very promising candidate because of its significantly lower cost compared to the Li-ion one, a very modest environmental impact of the materials,[8] and a remarkably high theoretical energy density. Indeed, the Li/O_2 electrochemical conversion process involves the exchange of more than one electron per formula-unit both during discharge and during charge, throughout reduction and

Received: September 21, 2020
Accepted: November 9, 2020
Published: November 30, 2020

https://dx.doi.org/10.1021/acsaem.0c02331
ACS Appl. Energy Mater. 2020, 3, 12263–12275

oxidation of various intermediate species,[9] with a theoretical capacity of 1200 mA h g^{-1} referred to the mass of oxygen and lithium in the formal reaction $2Li + O_2 \rightleftarrows Li_2O_2$, occurring at 2.9 V *versus* Li^+/Li.[10] Unlikely, safety issues related to the use of the lithium metal at the anode,[11,12] a complex mechanism of the oxygen reduction reaction (ORR),[13] the reactivity of the intermediates with the electrolytes,[14] and the insulating character of the Li_2O_2 leading to a high polarization of the oxygen evolution reaction (OER)[15] hindered the full development of this intriguing energy storage system. The reactive lithium can in fact decompose the common solutions and form an irregular solid electrolyte interphase (SEI) layer, which may promote the formation of dendritic structures during charge leading to short circuit of the cell, and possible thermal runaway in the presence of flammable organic solvents. Hence, the use of alkali metal anodes has been reconsidered in view of the development of alternative electrolytes with an enhanced safety content such as gels,[16] solid polymers,[17−19] and lowly flammable liquid solutions.[20] Among the liquid electrolytes, the end-capped glymes with ether chains of variable length $[CH_3O(CH_2CH_2O)_nCH_3]$ dissolving lithium salts[21−23] represent a suitable candidate for allowing reversible Li^+ ion exchange between the electrodes, with limited side reactions and acceptable stability in lithium metal batteries.[24,25] Recent studies have demonstrated the safe applicability of glyme-based electrolytes in lithium−air batteries[26] operating by above-mentioned reversible formation and dissolution of Li_2O_2 due to their low flammability and the relative stability toward radical species such as lithium superoxide (LiO_2) formed during ORR in the Li/O_2 cell,[9] while electrolytes based on organic carbonates commonly employed in lithium-ion batteries are flammable and easily decomposed during the electrochemical process.[27] Furthermore, the inclusion in the solution of a sacrificial additive such as vinylene carbonate,[28] $LiNO_3$,[29] and $Mg(NO_3)_2$,[30] that form a stable SEI at the lithium metal surface, was considered to be a very promising strategy to hinder the formation of lithium dendrites and optimize the electrolytes.[31,32] This favorable phenomenon has been widely exploited for avoiding the chemical process of the dissolved polysulfide intermediates with the Li metal in the Li−S battery.[33−36] In fact, the concomitant reduction of the additive along with the partial electrolyte decomposition consolidate the SEI and limit the direct contact and reactivity of the metal anode with the solution components.[33−35] Moreover, recent studies suggested the addition of $LiNO_3$ to the electrolyte as a suitable strategy to decrease the polarization of the ORR/OER electrochemical process in lithium−oxygen batteries,[37,38] while relevant performances have been achieved through the employment of molten $LiNO_3$ without a solvating agent.[39] In this regard, an interesting field of research for lithium metal batteries was represented by the use of electrolytes based on solutions with high concentrations of lithium salts, that is, solvent-in-salt configurations, which can lead to notable cycling efficiency and high specific capacity because of the formation of an improved and stable SEI layer, providing at the same time a suitable safety content.[40−43] We have investigated in this work the performances of lithium−oxygen batteries using electrolyte solutions consisting of diglyme [diethylene-glycol dimethyl-ether (DEGDME)] and triglyme [triethylene-glycol dimethyl-ether (TREGDME)] with a relevant amount of lithium salts [lithium bis(trifluoromethanesulfonyl)imide (LiTFSI) and $LiNO_3$]. The exploited salt amount approached the saturation limit of the solvents in order to achieve highly concentrated solutions with increased safety content and limited evaporation, thus favoring practical applications of the Li/O_2 cell in an open environment. Prior to use in a Li/O_2 cell, various techniques have been employed to fully characterize the electrolytes in terms of chemical and electrochemical properties, thermal stability, and chemical composition of the SEI film formed at the lithium metal surface. Throughout suitable analysis, this work sheds light on the adverse effects of electrolyte volatility during the operation in the open environment of the lithium−oxygen battery and suggests alternative solutions for achieving practical and safe applications of such a challenging energy storage system.

EXPERIMENTAL SECTION

LiTFSI ($LiN(SO_2CF_3)_2$, Sigma-Aldrich) and lithium nitrate ($LiNO_3$, Sigma-Aldrich) salts were dissolved by magnetic stirring overnight at room temperature in either DEGDME ($CH_3O(CH_2CH_2O)_2CH_3$, Sigma-Aldrich) or TREGDME ($CH_3O(CH_2CH_2O)_3CH_3$, Sigma-Aldrich) solvents in a ratio of 1.5 mol of each salt in 1 kg of DEGDME and 2 mol of each salt in 1 kg of TREGDME. The salts used for the electrolyte preparation were previously heated at 110 °C under vacuum for 24 h to remove traces of water, while the solvents were dried with molecular sieves (3 Å, Sigma-Aldrich) until a water content below 10 ppm was obtained, as verified by 899 Karl Fischer Coulometer, Metrohm. The obtained highly concentrated electrolytes will be subsequently indicated by the acronyms DEGDME_HCE and TREGDME_HCE, respectively. It is worth mentioning that the difference between the concentrations used in the two electrolytes is because of the different solubility of the salts in DEGDME and TREGDME, that is, higher in the latter than in the former.

X-ray photoelectron spectroscopy (XPS) measurements were carried out on lithium foils previously soaked in the electrolytes for 2 days inside an Ar-filled glovebox (MBraun, O_2 and H_2O content below 1 ppm) to allow SEI film formation and then dried under vacuum for 3 h in order to remove the electrolyte. The XPS response was obtained under vacuum (10^{-5} mbar) by using a PHOIBOS HSA3500 150 R6 spectrometer exploiting monochromatic Al Kα radiation (250 W) and a multichannel detector. Depth-profile data of the lithium sample surface were obtained by Ar^+ etching (acceleration voltage of 2.7 kV) at various sputtering times, that is, 0, 60, 120, 300, and 600 s.

Thermogravimetric analysis (TGA) was performed on DEGDME_HCE, TREGDME_HCE, DEGDME, TREGDME, LiTFSI, and $LiNO_3$ samples by increasing temperature from 25 to 800 °C with a rate of 5 °C min^{-1} in nitrogen flow through a Mettler Toledo-TGA/DSC. The weight loss of the DEGDME_HCE and TREGDME_HCE electrolytes under ambient environment was also checked at room temperature upon prolonged exposure to air for estimating their volatility in view of the application in the lithium−oxygen cell. The samples were stored in 25 mL beakers, and the weight values were collected through a Gibertini E42-B analytical balance that allowed measurements with a relative error lower than 3%.

The electrochemical measurements reported below were carried out by using CR2032 coin-type cells (MTI Corp.) assembled in an Ar-filled glovebox (MBraun, O_2 and H_2O content below 1 ppm).

The ionic conductivity of DEGDME_HCE and TREGDME_HCE was determined by electrochemical impedance spectroscopy (EIS) performed upon scan from room temperature to about 76 °C in symmetrical stainless-steel/electrolyte/stainless-steel cells employing an O-ring spacer (CS Hyde, 23-5FEP-2-50) with a 10 mm internal diameter and thickness of 127 μm to fix the cell constant at 0.0162 cm^{-1}. The impedance spectra were recorded by using a VersaSTAT MC Princeton Applied Research (PAR, AMETEK) instrument applying an alternate voltage signal of 10 mV in a frequency range between 500 kHz and 100 Hz.

The properties and the performances of the electrolytes in lithium cells were investigated by employing lithium disks with a 14 mm

https://dx.doi.org/10.1021/acsaem.0c02331
ACS Appl. Energy Mater. 2020, 3, 12263−12275

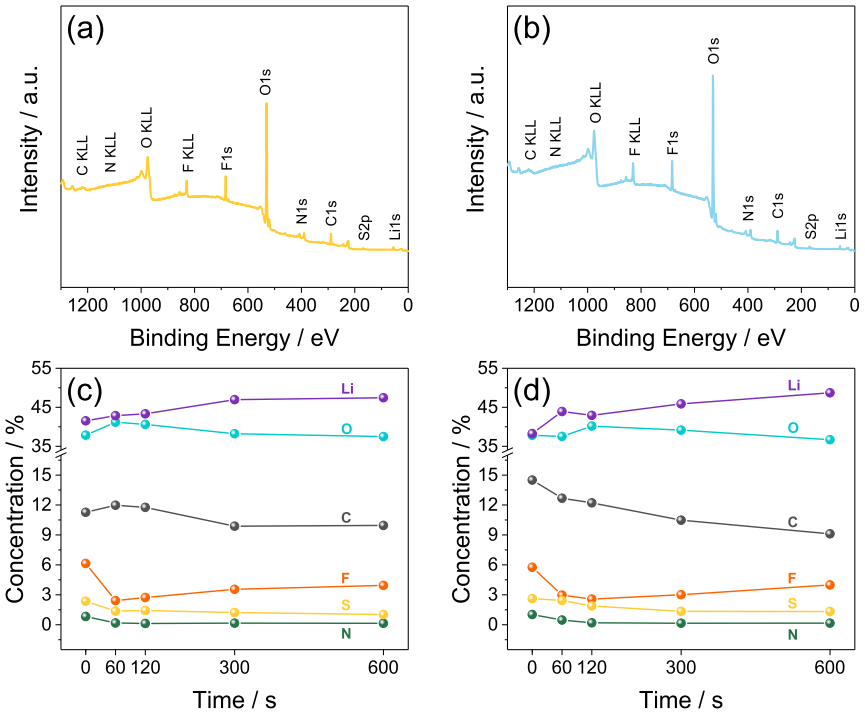

Figure 1. (a,b) X-ray photoelectron survey spectra recorded after 600 s of Ar^+ sputtering and (c,d) percent elements content detected upon Ar^+ etching of the surface of lithium foils soaked for 2 days with either (a,c) DEGDME_HCE or (b,d) TREGDME_HCE. The percent content was obtained by fitting of the survey spectra reported in Figure S1a,b for DEGDME_HCE and TREGDME_HCE, respectively.

diameter as electrodes and GF/A glass fiber (Whatman) 16 mm disks soaked with either DEGDME_HCE or TREGDME_HCE as separators.

The Li^+ transference number of DEGDME_HCE and TREGDME_HCE was determined through the Bruce–Vincent–Evans method.[44] A chronoamperometric test was performed on symmetrical Li/electrolyte/Li cells by applying a voltage of 30 mV for 90 min, and impedance spectra were recorded by EIS before and after polarization using a signal of 10 mV in the 500 kHz to 100 mHz frequency range. The Li^+ transference number values were then calculated through eq 1[44]

$$t^+ = \frac{i_{ss}}{i_0}\frac{\Delta V - R_0 i_0}{\Delta V - R_{ss} i_{ss}} \quad (1)$$

where i_0 and i_{ss} are the current values at the initial and steady state, respectively, ΔV is the applied voltage, R_0 and R_{ss} are the interphase resistance values before and after cell polarization, respectively, calculated from the impedance spectra. Both the chronoamperometric and the EIS measurements were carried out by using a VersaSTAT MC Princeton Applied Research (PAR, AMETEK) instrument.

The electrochemical stability of the electrolytes was evaluated through a lithium stripping-deposition test by means of galvanostatic cycling, where a current of 0.1 mA cm^{-2} was applied to Li/electrolyte/Li symmetrical cells using a MACCOR Series 4000 battery test system.

The Li/electrolyte interphase resistance was analyzed by EIS upon aging of symmetrical Li/Li cells employing either DEGDME_HCE or TREGDME_HCE. The spectra were recorded with a VersaSTAT MC Princeton Applied Research (PAR, AMETEK) instrument by applying a 10 mV signal in the 500 kHz to 100 mHz frequency range.

The electrochemical stability window of the electrolytes was evaluated through cyclic voltammetry (CV) in the cathodic region in the 0.01–2 V *versus* Li^+/Li potential range and through linear sweep voltammetry (LSV) in the anodic region from the open-circuit voltage (OCV) condition to 5 V *versus* Li^+/Li. The tests were carried out in cells employing a lithium anode, either DEGDME_HCE or TREGDME_HCE, and carbon as the working electrode, which was coated on copper or an aluminum current collector to perform the measurement in the cathodic or anodic region, respectively. The anodic region was further investigated by a chronoamperometry test in the 4.0–4.6 V *versus* Li^+/Li potential range. Prior to the experiment, a LSV scan was performed from the OCV to 3.9 V *versus* Li^+/Li, then the cell was held at 4 V for 1 h, and the potential was subsequently increased by using steps of 0.1 V every hour until 4.6 V while the current was measured during each step of chronoamperometry. The carbon working electrodes were prepared by doctor blade casting on the corresponding current collector of a slurry formed by Super P carbon (SPC, Timcal) and polyvinylidene fluoride (PVDF 6020, Solef Solvay) binder in a weight ratio of 90:10, dispersed in *N*-methyl-2-pyrrolidone (Sigma-Aldrich) solvent. The slurry was dried at 70 °C under air for 3 h and cut into 14 mm disks, and the resulting electrodes were subsequently dried at 110 °C under vacuum overnight to remove possible traces of water or solvent. The voltammetry tests were performed by employing a scan rate of 0.1 mV s^{-1} through a VersaSTAT MC Princeton Applied Research (PAR, AMETEK) instrument.

The electrolytes were then employed in Li/O_2 cells using top-meshed CR2032 coin-type cells into glass tubes sealed in a glovebox (MBraun, O_2 and H_2O content below 1 ppm) and subsequently filled with pure oxygen. The lithium–oxygen cells employed a 14 mm lithium disk as the anode and a 16 mm SPC electrode at the cathode side. The SPC electrodes for the Li/O_2 battery were prepared with the same procedure reported above, except for the current collector which consisted of a porous GDL foil (35BC, SiGracet). A SPC loading between 0.65 and 1.05 mg cm^{-2} was used in the Li/O_2 cells.

The stability of the electrolytes in lithium–air cells was investigated by means of EIS measurements upon aging at the open-circuit condition (OCV) through a VersaSTAT MC Princeton Applied Research (PAR, AMETEK) instrument by applying a 10 mV signal in the 500 kHz to 100 mHz frequency range.

All abovementioned impedance spectra recorded by EIS were fitted using the non-linear least squared (NLLS) method to obtain the resistance values. The fitting was performed through a Boukamp tool taking into account only fits with a χ^2 of the order of 10^{-4} or lower.[45,46]

https://dx.doi.org/10.1021/acsaem.0c02331
ACS Appl. Energy Mater. 2020, 3, 12263–12275

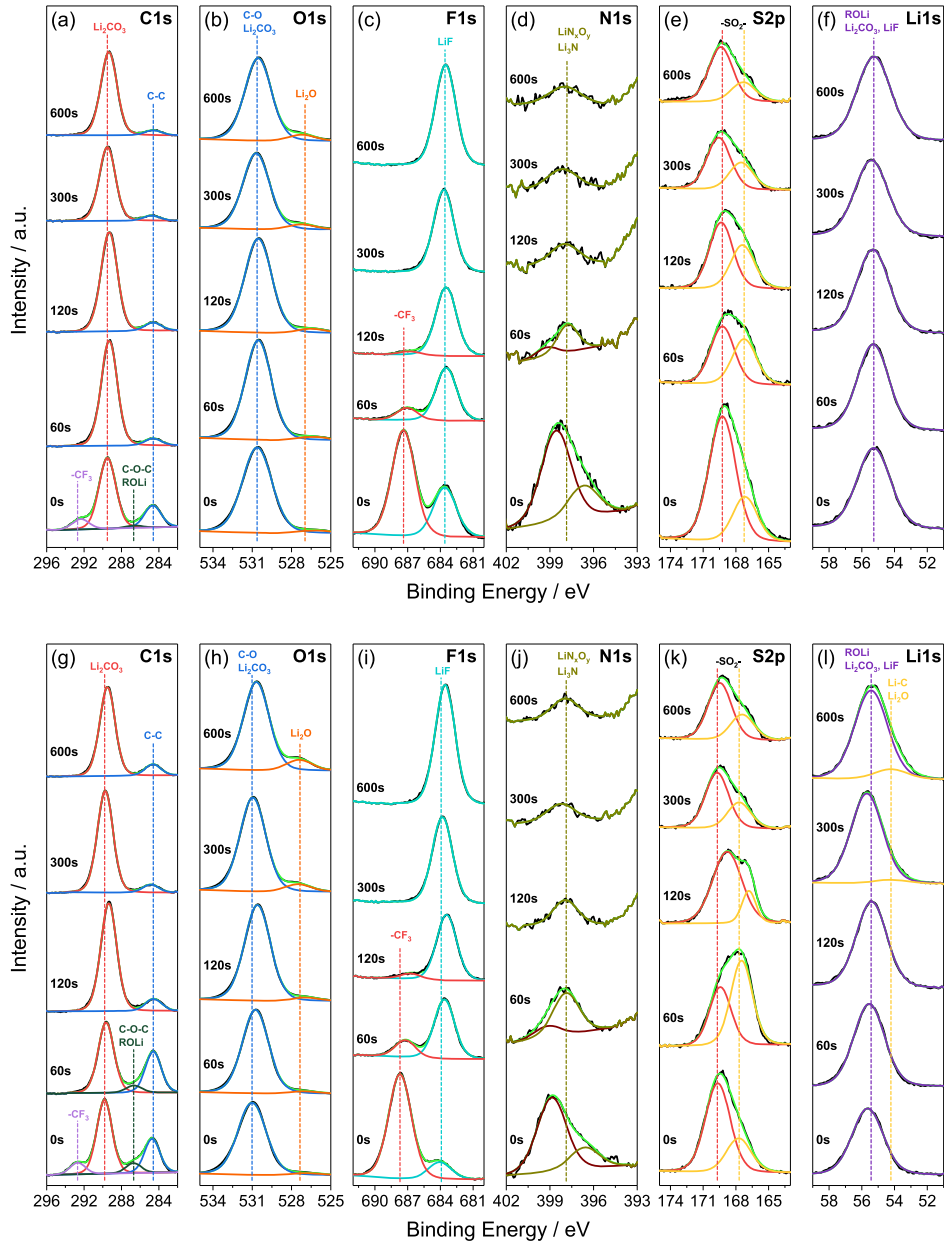

Figure 2. Deconvoluted XPS spectra of C 1s, O 1s, F 1s, N 1s, S 2p, and Li 1s for (a–f) DEGDME_HCE and (g–l) TREGDME_HCE at various times of Ar^+ sputtering on lithium foil surfaces aged in contact with the electrolytes for 2 days. The related survey spectra are reported in the Supporting Information in Figure S1a for DEGDME_HCE and S1b for TREGDME_HCE.

The performances of the lithium–oxygen cells employing DEGDME_HCE and TREGDME_HCE were evaluated by galvanostatic cycling using a MACCOR Series 4000 battery test system. The measurements were carried out by applying a current of 100 mA g^{-1}, referred to the SPC mass, in the 1.5–4.6 V voltage range with a step time of 5 or 10 h, in order to limit the delivered specific capacity to 500 and 1000 mA h g^{-1}, respectively.

RESULTS AND DISCUSSION

As mentioned in the previous section, the formation of a SEI layer at the lithium anode by partial reduction of the electrolyte and concomitant passivation of the metal surface is widely considered to be the key factor for ensuring the electrode stability in the battery and limiting the formation of dendritic structures that can lead to short circuits and cell failure.[32] On the other hand, the actual role of the SEI is still an open point which may be further clarified by the study of the chemical nature of the species formed at the electrode surface,[47] in particular in new classes of electrolytes such as those used in the Li/O_2 battery, including glyme-based solutions.[26] Therefore, Figure 1 investigates the SEI composition at an increasing depth of lithium metal foils soaked into DEGDME_HCE and TREGDME_HCE solutions by means of XPS performed upon Ar^+ sputtering at various times, that is, 0, 60, 120, 300, and 600 s, to etch the passivation layer (see the Experimental Section for further details). Figure 1a,b shows the survey spectra recorded after 600 s for DEGDME_HCE and TREGDME_HCE, respectively, while the time evolution of the spectra is reported in Figure S1 in the Supporting Information. The binding energies of the curves reveal that the SEI layer is mainly composed by C, O, F, N, S, and Li (see the detailed identification in Figure 2), as indeed expected by the components of the electrolytes (see the Experimental Section),

https://dx.doi.org/10.1021/acsaem.0c02331
ACS Appl. Energy Mater. 2020, 3, 12263–12275

Table 1. Percent Elements Content Determined by XPS[a]

electrolyte	sputtering time (s)	C (%)	O (%)	F (%)	N (%)	S (%)	Li (%)
DEGDME_HCE	0	11.27	37.87	6.14	0.82	2.36	41.54
	60	11.98	41.19	2.42	0.17	1.36	42.87
	120	11.76	40.61	2.73	0.13	1.43	43.33
	300	9.88	38.24	3.55	0.16	1.22	46.96
	600	9.95	37.49	3.94	0.14	1.03	47.46
TREGDME_HCE	0	14.5	37.83	5.76	1.02	2.62	38.27
	60	12.68	37.53	2.97	0.47	2.43	43.92
	120	12.22	40.2	2.57	0.19	1.88	42.95
	300	10.48	39.16	3.01	0.15	1.34	45.88
	600	9.11	36.71	3.99	0.16	1.32	48.72

[a]The data are obtained by fitting of the X-ray photoelectron survey spectra reported in Figure S1a,b in the Supporting Information, recorded at various times of Ar^+ sputtering carried out on the surface of lithium foils soaked for 2 days with either DEGDME_HCE or TREGDME_HCE, respectively. The corresponding trends *vs* time are depicted in Figure 1c,d, respectively.

namely, the poly-ether chains of the organic solvents, the LiTFSI, and the $LiNO_3$ salts. The analysis of the above XPS data, reported in Table 1 and plotted in Figure 1c,d, reveals that the percent of the various elements changes upon surface etching, that is, by increasing the Ar^+ sputtering time, and likely indicates a different composition of outer layers of the SEI over the lithium with respect to the inner ones for both DEGDME_HCE (Figure 1c) and TREGDME_HCE (Figure 1d).

It is worth noting that Li has the most relevant contribution to the XPS signal because of its metallic nature, followed by O which is contained in all the species forming the electrolytes. Furthermore, SEI-film etching slightly increases the Li signal as expected by the progressive exposure of the metal surface, while only minor fluctuations are observed for oxygen. The decrease of the C content by etching (Figure 1c,d and Table 1 at increasing times) suggests for both electrolytes a higher content of side species such as lithium carbonate and lithium oxide in the inner side of the SEI compared to the outer side, possibly because of the remarkable reactivity of the fresh lithium surface.[31,32] On the other hand, the outer side of the SEI observed before etching (Figure 1c,d and Table 1 at t = 0 s) reveals the highest concentration of S, N, and F likely due to the preferential precipitation of $LiNO_3$ and LiTFSI salts. In spite of a continuous decrease of S and N contents by etching, the F content initially decreases and subsequently increases, thus suggesting the formation of fluorinated precipitates such as LiF in the inner side of the SEI in proximity of the metallic surface.[48]

Further insights into the actual SEI composition are provided by the deconvoluted XPS responses referred to the various elements for DEGDME_HCE (Figure 2a–f) and TREGDME_HCE (Figure 2g–l). The C 1s signals (Figure 2a,g) show a decreasing intensity upon etching of the peaks with binding energies of 284.6 and 286.7 eV, related to C–C and C–O–C or ROLi bonds,[29,49] respectively, and a concomitant increase of the intensity of the lithium carbonate Li_2CO_3 related peak at 289.6 eV.[50,51] A certain contribution to the carbon signal of LiTFSI salt cannot be completely excluded, however without significantly altering the qualitative evaluation of the results. This trend further suggests the predominant presence of Li_2CO_3 in the inner side of the SEI (t = 600 s), as already mentioned during discussion of Figure 1c,d, and indicates the precipitation in the outer SEI side of species characterized by organic C–C, C–O–C, and $-CF_3$ bonds (t = 0 s).[52] In addition, a more intense signal at 286.7 eV (C–O–C, ROLi) for TREGDME_HCE (Figure 2g) compared to DEGDME_HCE (Figure 2a) suggests a bigger contribution to the SEI of the solvent with the longer ether chain. It is worth noting that the C 1s signal at 292.6 eV of the $-CF_3$ groups because of LiTFSI salt[49] can be observed only at the initial stage before SEI etching for both electrolytes (Figure 2a,g), thus suggesting possible lithium salt deposition at the outer SEI. This is likely confirmed by the F 1s signal (Figure 2c,i) in which the peak between 687 and 688 eV, assigned to $-CF_3$,[53] progressively vanishes by surface etching; concomitantly, the same panels reveal the increase of the peak at 683.6 eV and account for the formation of LiF due to salt decomposition on the lithium surface, particularly in the inner side of the SEI.[47] LiTFSI can also be associated to the broad S 2p signal (Figure 2e,k) between 164 and 173 eV, which decreases by etching, and can be resolved in two peaks ascribable to the S $2p_{3/2}$ and S $2p_{1/2}$ doublet of the $-SO_2-$ group,[54] without excluding the possible formation of sulfur compounds with various oxidation states by reduction of the salt.[55] Moreover, the convoluted N 1s signals (Figure 2d,j) between 394 and 401 eV, that merge into one after 120 s of etching, may likely account for the formation of negatively charged nitrogenous species, such as Li_3N (N^{3-}), and, more in general, LiN_xO_y,[29] by the reduction of the $LiNO_3$ as well for the imide groups of LiTFSI salt.[53,55] On the other hand, the O 1s (Figure 2b,h) and Li 1s (Figure 2f,l) signals can actually identify the expected C–O bond and Li_2CO_3 at 531 eV, and ROLi species around 55 eV,[29,56] respectively, while the growth of the peaks at 527 eV by etching the samples (Figure 2b,h) suggests the presence of Li_2O at the inner side of the SEI,[29,57] which is expected by the unavoidable partial oxidation of the lithium metal surface.

A further signal for TREGDME_HCE at 54.2 eV (Figure 2l) may account for the presence of Li–C bonds[29,57] while possible contribution of LiF around 56.5 eV[53] and Li_2CO_3 at about 55.5 eV[58] to the broad Li 1s signal cannot be excluded. Overall, the XPS evidences the formation of a complex SEI on the lithium surface which is mainly composed of inorganic species, such as LiF, Li_2CO_3, Li_3N, LiN_xO_y, and Li_2O, in the inner side near by the reactive metal, and organic solvent reduction products, such as ROLi and ROR as well as precipitated salts (*e.g.*, LiTFSI), in the outer side. Indeed, the features of the SEI formed by DEGDME_HCE and TREGDME_HCE at the lithium surface can actually indicate possible applications of the electrolyte in efficient and stable batteries.

https://dx.doi.org/10.1021/acsaem.0c02331
ACS Appl. Energy Mater. 2020, 3, 12263–12275

The thermal stability of electrolytes and solution components is investigated by TGA in view of possible applications in the Li/O_2 battery. It is worth mentioning that TEGDME has already shown suitable stability and applicability in Li/O_2 cells.[14,26] Herein we study shorter glymes, that is, DEGDME and TREGDME, with significantly different volatility.[27] A comparison between DEGDME, TREGDME, and TEGDME in terms of some chemical and physical properties is reported in Table S1 in the Supporting Information. Figure 3 compares

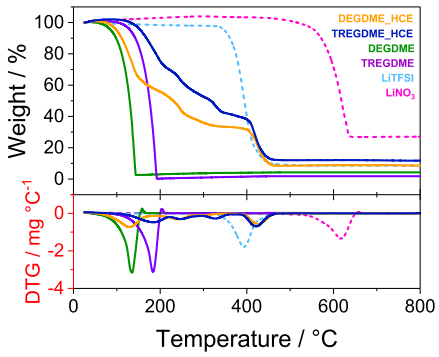

Figure 3. TGAs (black left-*y* axis) and corresponding differential curves (DTG, red left-axis) of DEGDME_HCE (orange), TREGDME_HCE (blue), DEGDME solvent (green), TREGDME solvent (violet), LiTFSI (light blue, dashed), and $LiNO_3$ (pink, dashed). Temperature range: 25−800 °C; heating rate: 5 °C min^{-1}.

the responses of the two electrolytes with those of DEGDME and TREGDME solvents as well as LiTFSI and $LiNO_3$ salts, both in terms of weight loss (TGA, top panel) and corresponding differential curves (DTG, bottom panel). It is worth noting that the weight loss due to evaporation observed for DEGDME (green) and TREGDME (violet) begins at around 50 and 100 °C, respectively, while the one associated to the corresponding electrolytes occurs at 80 °C for DEGDME_HCE (orange) and 130 °C for TREGDME_HCE (blue). The remarkable boiling point elevation observed above may be likely ascribed to the relevant presence of lithium salts into the electrolyte formulation.[59] Furthermore, the longer glyme chain in TREGDME solvent compared with DEGDME is actually reflected into a lower volatility for TREGDME_HCE electrolyte compared to DEGDME_HCE[60] and consequently into a higher safety content and applicability in an open environment such as the one expected for the Li/O_2 cell. The multiple weight loss observed between 200 and 400 °C for the two electrolytes can be ascribed to the removal of the glyme from crystallized salt−solvent complexes which are principally promoted by the strong interaction between the oxygen atoms in the ether chains and the Li^+ ions rather than the anions.[61] Therefore, the degradation of the glyme−salt complexes by solvent evaporation occurs throughout a multiple-step dry-recrystallization mechanism leading to the bare lithium salts, that is, LiTFSI and $LiNO_3$.[49,62] Further weight loss above 400 °C indicates LiTFSI salt degradation (compare plain blue and orange TGA curves with the light blue dashed-curve related to the above salt shown in Figure 3), while $LiNO_3$ degradation expected around 600 °C (the pink dashed-curve shown in Figure 3) is not observed or kinetically slowed down. The missing degradation of $LiNO_3$ until 800 °C is also confirmed by TGA residues of about 9% for DEGDME_HCE and 11% for TREGDME_HCE which can be obtained only by taking into account the presence of the above salt.

The ionic conductivity, that is, a key factor for the electrolyte applicability, is determined by means of EIS measurements performed during the scan from room temperature to around 76 °C, while the corresponding Arrhenius plots are displayed in Figure 4a (see the related Nyquist plots in Figure S2a,b in the Supporting Information). The data of Figure 4a reveal that TREGDME_HCE (blue) has lower conductivity with respect to DEGDME_HCE (orange), with values ranging from 8.9×10^{-4} S cm^{-1} at room temperature to 2.5×10^{-3} S cm^{-1} at 76 °C for the former and from 3.3×10^{-3} to 7.8×10^{-3} S cm^{-1} for the latter. This experimental response may be partially justified by an easier mobility of the ions in DEGDME_HCE compared to TREGDME_HCE which has in turn a more relevant concentration of the lithium salts and a longer polyether chain of the glyme solvent, thus a higher viscosity.[63] On the other hand, both electrolytes exhibit conductivity values approaching or even higher than 10^{-3} S cm^{-1}, thereby matching the requirement for electrochemical applications. Subsequently, the electrolytes were investigated in the symmetrical Li/Li cell to determine the Li^+ transference number (t^+) according to the Bruce−Vincent−Evans method (see the Experimental Section).[44] Table 2 reports the parameters used in eq 1 while the chronoamperometric curves and the Nyquist plots related to the EIS measurements are reported in Figure S2c,d in the Supporting Information. The t^+ values reported in Table 2 and depicted in Figure 4a (inset) imply that the higher viscosity and salt concentration of TREGDME_HCE compared to DEGDME_HCE reflect into a lower Li^+ ion transport and transference number (*i.e.*, 0.51 for the former and 0.60 for the latter). On the other hand, the obtained t^+ values appear adequate for applications in lithium cells and comparable with those usually ascribed to glyme electrolytes.[64]

The electrochemical stability of the two electrolytes is investigated by prolonged lithium stripping/deposition throughout galvanostatic cycling in the symmetrical Li/Li cell reported in Figure 4b. Initially, DEGDME_HCE (orange) and TREGDME_HCE (blue) exhibit overvoltage values of 135 and 175 mV that decrease to 30 and 75 mV, respectively, after 70 h of measurement and subsequently stabilize around the latter values. The observed decrease of the overvoltage is likely due to a partial dissolution of the SEI film which is formed at the lithium surface after cell assembly, while the final stabilization indicates the consolidation of the abovementioned SEI which may actually allow the prolonged cycling of the lithium cells without any further side reaction.[49] The chemical stability of the electrolytes is instead investigated by EIS measurements, carried out upon prolonged aging of Li/Li symmetrical cells. It is worth noting that all the recorded Nyquist plots, reported in Figure S3 in the Supporting Information, can be suitably represented by the $R_e(R_1Q_1)$-(R_2Q_2) equivalent circuit, where R_e is the electrolyte resistance, (R_1Q_1) element accounts for the charge transfer at the electrode/electrolyte interphase and the SEI layer (high-middle frequency semicircle), and (R_2Q_2) represents a Warburg-type Li^+ ion diffusion (low-frequency semicircle).[32] Interestingly, during the initial 14 h upon cell assembly the DEGDME_HCE (Figure S3a and Table S2 in the Supporting Information) exhibits slightly higher values of the interphase resistance with respect to TREGDME_HCE (Figure S3b and Table S3 in the Supporting Information). Furthermore, the

https://dx.doi.org/10.1021/acsaem.0c02331
ACS Appl. Energy Mater. 2020, 3, 12263−12275

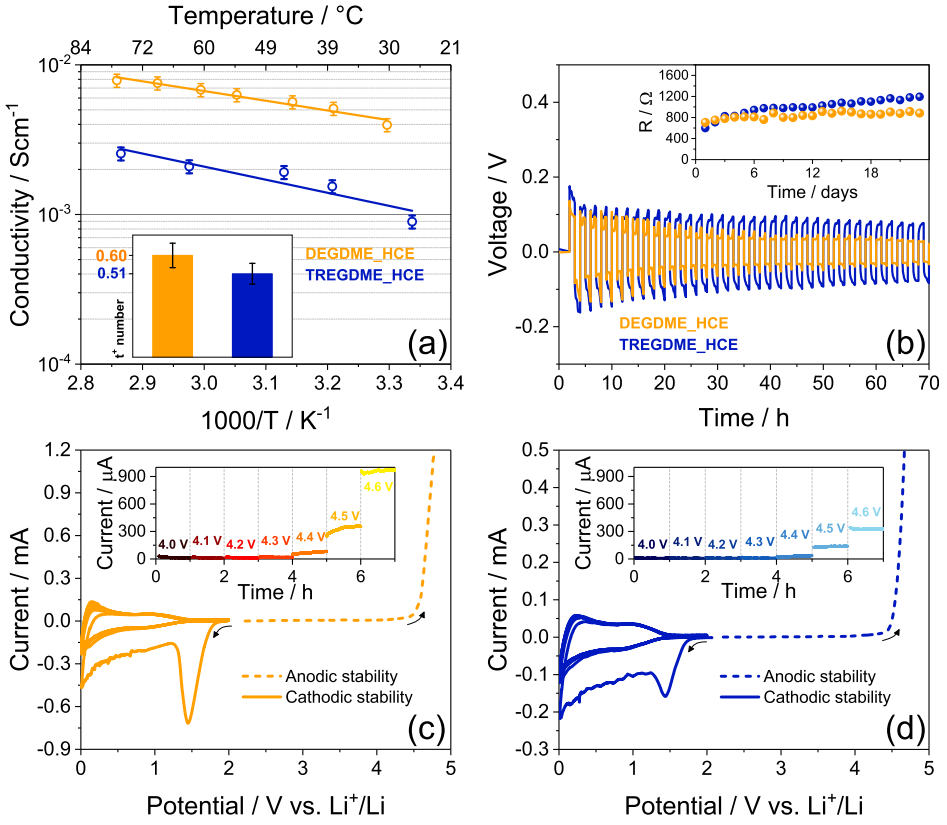

Figure 4. (a) Arrhenius conductivity plots and Li^+ transference number values (inset, see the determination method in the Experimental Section) of DEGDME_HCE (orange) and TREGDME_HCE (blue). (b) Lithium stripping/deposition tests performed on Li/electrolyte/Li symmetrical cells employing either DEGDME_HCE (orange) or TREGDME_HCE (blue) by applying a current of 0.1 mA cm^{-2}; inset shows the interphase resistance trends recorded upon Li/electrolyte/Li symmetrical cells aging employing DEGDME_HCE (orange) or TREGDME_HCE (blue) through EIS in the 500 kHz to 100 mHz frequency range by applying a signal of 10 mV (see the corresponding Nyquist plots in Figure S3 and the related NLLS analyses in Tables S1 and S2 in the Supporting Information). (c,d) Electrochemical stability window determined by means of CV in the cathodic region (solid line) and LSV in the anodic one (dashed line) performed on lithium cells employing either (c) DEGDME_HCE or (d) TREGDME_HCE, and SPC as the working electrode; scan rate: 0.1 mV s^{-1}, CV potential range: 0.01−2 V *vs* Li^+/Li; insets show the chronoamperometry test carried out in the 4.0−4.6 V *vs* Li^+/Li potential range through voltage increase by steps of 0.1 V every hour.

Table 2. Lithium Transference Number (t^+) of DEGDME_HCE and TREGDME_HCE and Parameters of Bruce−Vincent−Evans Equation (See Eq 1 in the Experimental Section)[a]

electrolyte	initial current (i_0) [A]	steady-state current (i_{ss}) [A]	initial resistance (R_0) [Ω]	steady-state resistance (R_{ss}) [Ω]	Li^+ transference number (t^+)
DEGDME_HCE	4.16×10^{-4}	3.62×10^{-4}	56.3	56.2	0.60
TREGDME_HCE	9.89×10^{-5}	7.04×10^{-5}	166	156	0.51

[a]The resistance values are determined by NLLS analyses performed on the Nyquist plots of symmetrical Li/Li cells containing the electrolytes reported in Figure S2c,d in the Supporting Information, which also displays the chronoamperometric curves used to obtain the currents values before and after polarization. EIS frequency range: 500 kHz to 100 mHz; signal amplitude: 10 mV. Chronoamperometry was performed for 90 min by applying a voltage of 30 mV.

resistance trends related to the subsequent EIS measurements reported in the inset of Figure 4b and listed in Tables S1 and S2 reveal a less significant growth for DEGDME_HCE with respect to TREGDME_HCE, with steady-state values between 800 and 900 Ω after 10 days for the former, while a slight continuous increase over the whole test to the final value of 1194 Ω for the latter (see related Nyquist plots in Figure S3c,d, respectively). The different electrode/electrolyte interphase resistance trending observed for the two solutions likely suggests diverse stabilization kinetics of the SEI at the lithium surface because of their different composition in terms of solvent nature and salt contents, as actually indicated by the literature paper.[65] Afterward, the electrochemical stability window of the electrolytes is determined in lithium cells by means of LSV and CV to investigate the anodic and the cathodic regions, respectively, employing carbon as the working electrode. The obtained current *versus* potential curves displayed in Figure 4c,d for DEGDME_HCE and TREGDME_HCE, respectively, show similar trends. Indeed, the first CV cycle of the cells reveals in the cathodic region an irreversible peak centered at about 1.5 V *versus* Li^+/Li related to the $LiNO_3$ salt reduction[33] and a convoluted response extended down to 0.01 V *versus* Li^+/Li accounting for multiple processes such as the electrolyte decomposition with SEI formation, the insertion of Li^+ ions into the amorphous SPC, and their possible electrodeposition at the carbon electrode surface.[66] The subsequent well-overlapped profiles exhibit reversible broad peaks at about 1 V and 0.01 V *versus* Li^+/Li

https://dx.doi.org/10.1021/acsaem.0c02331
ACS Appl. Energy Mater. 2020, 3, 12263−12275

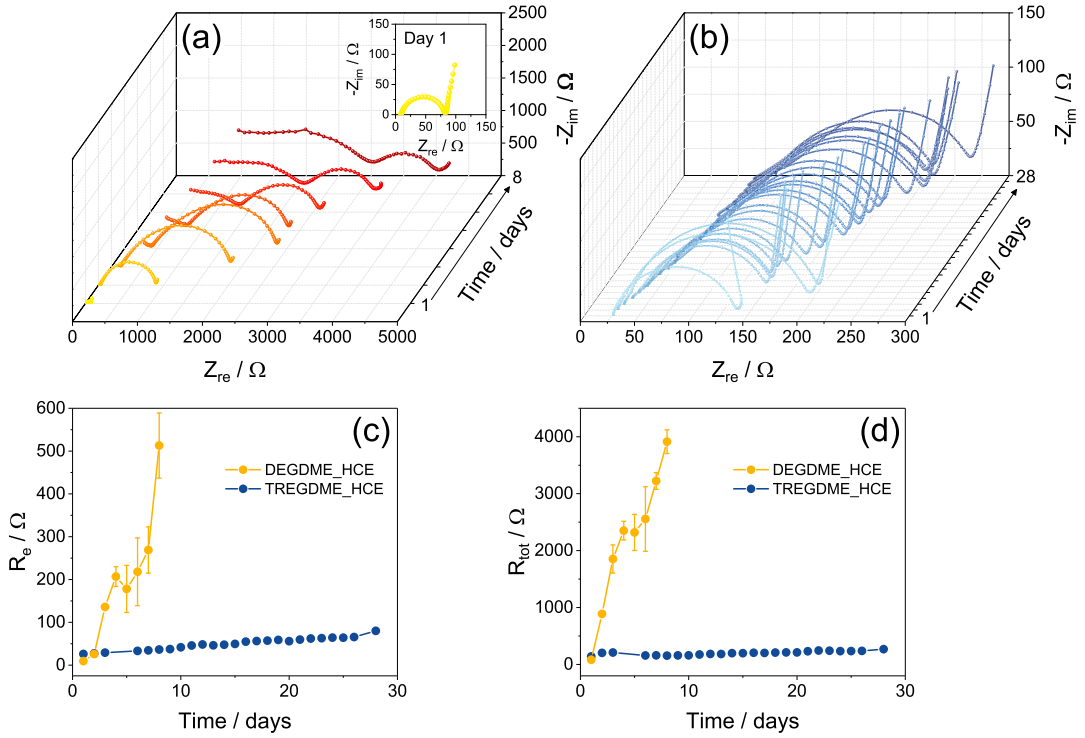

Figure 5. (a,b) Nyquist plots recorded by EIS upon aging of lithium−oxygen cells employing (a) DEGDME_HCE and (b) TREGDME_HCE in the Li/electrolyte/SPC-O_2 configuration; inset in panel (a) shows magnification of the impedance spectrum at day 1 for DEGDME_HCE. (c,d) Trends of (c) the electrolyte resistance (R_e) and (d) the total electrode/electrolyte interphase resistance (R_{tot}), obtained by NLLS analyses performed on the Nyquist plots reported in panels (a,b). EIS frequency range: 500 kHz to 100 mHz; signal amplitude: 10 mV. The actual resistance values and the corresponding relative errors are reported in Tables S4 and S5 in the Supporting Information for DEGDME_HCE and TREGDME_HCE, respectively.

accounting for Li^+ (de)-insertion and electrodeposition processes, respectively.[66] On the other hand, the LSV scan performed in the anodic region reveals for both electrolytes the absence of significant reactions from the OCV condition until a potential of about 4.4 V *versus* Li^+/Li which instead runs the oxidative decomposition of the solutions, as effectually indicated by a relevant increase of the current value. Therefore, the electrochemical stability of the two electrolytes can be estimated to range from 0 to around 4.4 V *versus* Li^+/Li, that is, an appropriate range for applications in the lithium battery.[60] A more accurate evaluation of the anodic limit of the two solutions can be obtained by chronoamperometry at gradually raising potentials, that is, by steps of 0.1 V every hour from 4.0 to 4.6 V *versus* Li^+/Li. The responses of the cells using DEGDME_HCE and TREGDME_HCE, depicted in the insets of Figure 4c,d, respectively, reveal significant electrolyte oxidation at 4.4 V *versus* Li^+/Li for the former with a current of 90 μA and at 4.5 V *versus* Li^+/Li for the latter with a current of 130 μA. Further increase of the potential leads to more relevant electrolyte decomposition with currents of 350 and 960 μA at 4.5 and 4.6 V *versus* Li^+/Li, respectively, for the cell using DEGDME_HCE and of 330 μA at 4.6 V for the one using TREGDME_HCE. These results confirm for TREGDME_HCE an anodic stability of 4.4 V *versus* Li^+/Li and restrict the one of DEGDME_HCE to 4.3 V *versus* Li^+/Li. It is worth mentioning that both electrolytes reveal a sufficient anodic stability for operation in the lithium−oxygen battery,[10] in particular TREGDME_HCE which has lower degradation current and improved electrochemical stability.

The applicability of the electrolytes in the lithium−oxygen battery is preliminarily investigated by means of EIS upon aging of the Li/electrolyte/SPC cells in the O_2 atmosphere (see the Experimental Section for details on cell configuration). Panels a and b of Figure 5 show the Nyquist plots recorded for DEGDME_HCE and TREGDME_HCE, respectively, in the above lithium−oxygen cell. During the initial stage after cell assembly, the EIS shows a response for both cells characterized by the presence of one semicircle with resistance of about 74 and 115 Ω for DEGDME_HCE and TREGDME_HCE, respectively, attributed to the native film formed on the electrodes, in particular at the lithium surface, and an almost vertically tilted line representing the cell geometric capacity (see Tables S4 and S5 in the Supporting Information for the corresponding NLLS analyses). This response possibly suggests an almost blocking electrode behavior of the cells which hold at the OCV a potential of about 3.1 V and can be represented by the equivalent circuit $R_e(R_1Q_1)Q_g$.[45,46] During the subsequent days, both cells can be represented by a more complex equivalent circuit including additional R_iQ_i elements in series to take into account the modification of the electrode/electrolyte interphases including SEI film growth, partial dissolution, or possible degradation.[46] Figure 5c shows the time evolution of the electrolyte resistance (R_e, high-frequency intercept of the plots), while Figure 5d depicts the trend of the overall resistance (R_{tot}), as determined by the sum of R_e and the various R_i obtained by NLLS analyses in Tables S4 and S5. Relevantly, DEGDME_HCE (orange) reveals a very fast and remarkable increase of both R_e and R_{tot}, instead TREGDME_HCE (blue) evidences stable trend with only minor increase of the overall resistance value, and limited fluctuations mainly because of expected partial film modification and possible consolidation.[45,46] Indeed, the limited initial values of

https://dx.doi.org/10.1021/acsaem.0c02331
ACS Appl. Energy Mater. 2020, 3, 12263−12275

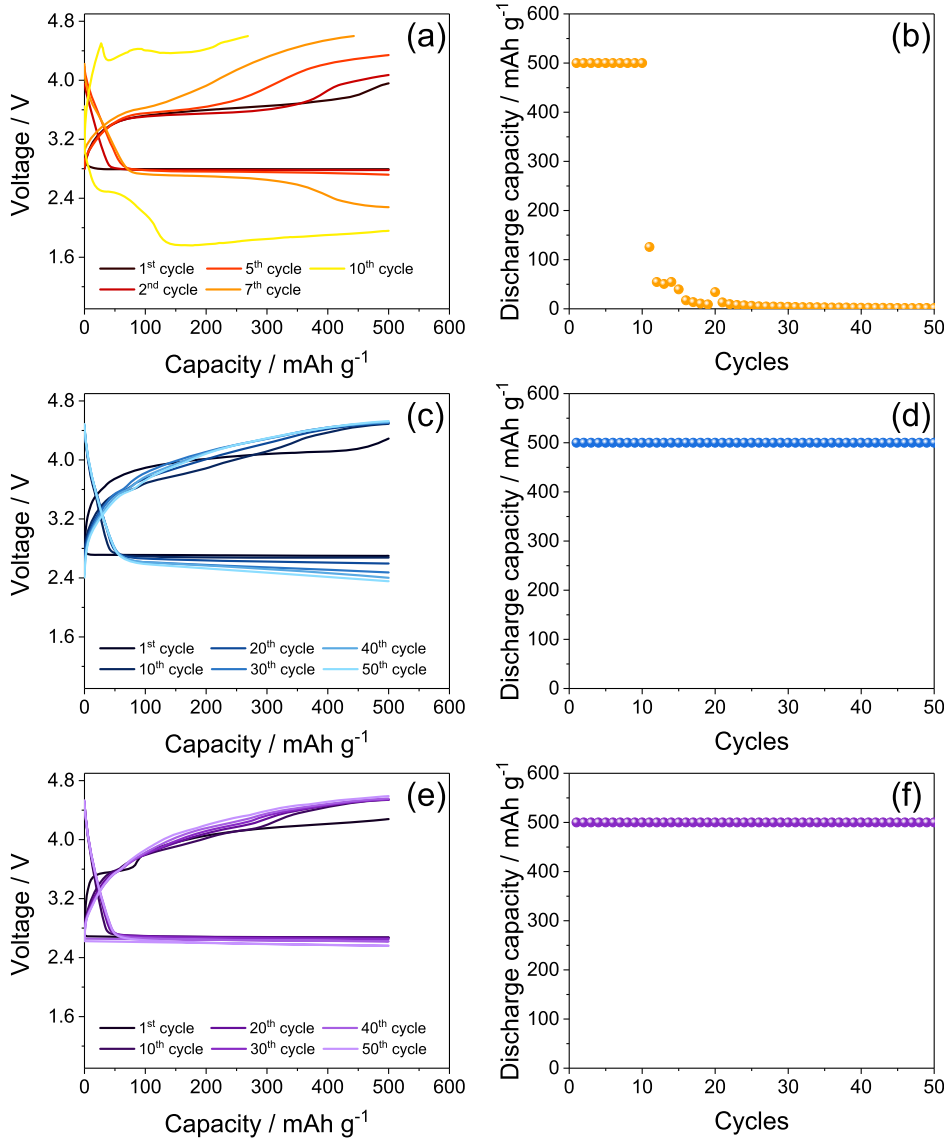

Figure 6. (a,c,e) Voltage profiles and (b,d,f) corresponding cycling trends of galvanostatic measurements performed by applying a constant current rate of 100 mA g^{-1} (referred to the SPC mass) to lithium−oxygen cells employing either (a,b) DEGDME_HCE or (c−f) TREGDME_HCE in the Li/electrolyte/SPC-O_2 configuration. Panels (a−d) show the performances of fresh cells, while panels (e,f) display the performances of a lithium−oxygen cell aged for 7 days prior to the test. Voltage range: 1.5−4.6 V. The specific capacity was limited to 500 mA h g^{-1}, referring to the SPC mass, by setting a step time of 5 h of discharge and charge. SPC loading: 0.65 mg cm^{-2} (SPC mass 1.3 mg, geometric electrode surface area 2 cm^2).

R_{tot} for DEGDME_HCE, that is, 83 Ω in Table S4, abruptly increases to about 900 Ω after 1 day and exceeds 1800 Ω after the 2nd, while the R_e concomitantly increases from about 9 to 26 Ω. This phenomenon, which leads to R_e and R_{tot} higher than 500 and 3900 Ω, respectively, after only 8 days of test may be most likely ascribed to a progressive degradation of the electrode/electrolyte interphase promoted by DEGDME solvent volatilization with formation of a grain boundary in the cell, as indeed suggested by the concomitant appearance and growth of an additional high-frequency semicircle in the related Nyquist plots (Figure 5a). This trend, which is usually observed for solid or crystalline electrolyte phases, indicates the presence of heterogeneity in the electrode/electrolyte interphase that can limit the Li^+ ion transport leading to poor performance of the lithium battery.[63] Instead, TREGDME_HCE displays an improved stability with respect to DEGDME_HCE, even though minor electrolyte volatilization cannot be excluded. The corresponding Nyquist plots in Figure 5b reveal modifications of the electrode/electrolyte interphase particularly during the initial 3 days, with an increase of R_e from about 26 to 29 Ω and R_{tot} from 141 to 209 Ω, while R_e and R_{tot} become 80 and 269 Ω, respectively, after 28 days of measurement (see Table S5 in the Supporting Information). Therefore, the lithium−oxygen cell employing TREGDME_HCE exhibits much lower values of the electrode/electrolyte interphase resistance with respect to DEGDME_HCE (compare Tables S4 and S5), thus suggesting suitable applicability of the former electrolyte in this class of energy storage systems. Moreover, the fluctuations of R_{tot} from 141 to 209 Ω after 3 days and down to 160 Ω after 7 days (Figure 5d) likely suggest the consolidation of the SEI layer and possibly the protection of the lithium anode.[67] As mentioned above, the different behaviors of the two electrolytes may be in part attributed to the lower volatility of TREGDME_HCE compared to DEGDME_HCE, already evidenced by the TGA in Figure 3. This aspect is further

https://dx.doi.org/10.1021/acsaem.0c02331
ACS Appl. Energy Mater. 2020, 3, 12263−12275

investigated in Figure S4 in the Supporting Information, which displays the weight % change of samples of DEGDME_HCE and TREGDME_HCE upon prolonged exposure to the ambient condition at the room temperature. The figure evidences that TREGDME_HCE weight (blue) fluctuates around 100% likely due to absorption and desorption of ambient moisture, which is instead avoided in the Li/O_2 cell studied herein, while DEGDME_HCE weight (orange) significantly decreases during the whole test to reach a final value approaching 65% of the initial one, thus suggesting much more relevant evaporation of the latter compared to the former.

Figure 6 displays the electrochemical performances of DEGDME_HCE and TREGDME_HCE in the lithium−oxygen cell, tested by means of galvanostatic cycling with capacity limited to 500 mA h g^{-1} with respect to the SPC mass, which is a capacity value suitable for preventing excessive nucleation of Li_2O_2 on the positive electrode surface (see the Experimental Section for details on the test conditions).[68] During the first cycle, the voltage profile of the cell employing DEGDME_HCE (Figure 6a) reveals relatively limited polarization, that is, of about 0.8 V, which however progressively increases and leads to complete cell failure after 10 cycles of charge/discharge, as also evidenced by the corresponding cycling trend in Figure 6b. This trend may be actually expected by taking into account the rapid increase of the Li/O_2 cell impedance during aging observed in Figure 5, which in turn increases the cell polarization above the operating voltage of the electrolyte (see Figure 4c) and leads to decomposition with cell degradation. Nonetheless, the limited polarization observed during the first cycle detected in Figure 6a, as well as the enhanced electrochemical characteristics of DEGDME_HCE observed in this work (see Figure 4), could suggest it for application in other types of lithium metal-based energy storage systems. The cell employing TREGDME_HCE, instead, reveals a remarkably different behavior both in terms of the voltage profile (Figure 6c) and cycling trend (Figure 6d). Despite a higher ORR/OER polarization during the first cycle (*i.e.*, of about 1.3 V) compared to DEGDME_HCE, which is likely ascribed to an electrochemical process kinetically limited by the lower conductivity and Li^+ transference number of TREGDME_HCE (Figure 4a), the cell using the latter electrolyte reveals a much more stable profile (compare Figures 6a and 6c) and an extended cycling trend (compare Figures 6b and 6d). However, the voltage profile of the cell using TREGDME_HCE shows a decrease of ORR voltage by cycling possibly because of the progressive modification of the SEI layer at the electrode surface by the ongoing test, as already observed by EIS measurements in Figure 5, which suggest additional few days of aging for achieving a steady-state condition. Therefore, taking into account the data of Figure 5d, we have set up a new cycling test on a Li/O_2 cell using TREGDME_HCE with same protocol used in the previous test, except for the aging time which is extended from few hours to 7 days. The data of the new test clearly reveal an enhanced stability of the ORR voltage profile at about 2.7 without significant signs of decrease (Figure 6e) during the 50 cycles taken into account (Figure 6f). This important result suggests the key role of the SEI layer at the lithium surface, which is herein improved by the presence of $LiNO_3$ and the high salt concentration, to achieve suitable operation of the Li/O_2 cell using a glyme-based electrolyte. Considering the ORR voltage (2.7 V) and the specific capacity referred to the SPC mass of 500 mA h g^{-1}, we may estimate for this cell a theoretical energy density of 1350 W h kg^{-1} and a practical value of 270 W h kg^{-1} which is achieved by taking in consideration a reduction factor of 1/5 to include inactive parts of the battery.[26] Further increase of the practical energy density of the battery may be achieved by raising the discharge time, as shown in Figure S5 in the Supporting Information by the voltage profile of a preliminary Li/TREGDME_HCE/SPC-O_2 cell galvanostatically cycled at the constant current rate of 100 mA g^{-1} where the specific capacity is limited to 1000 mA h g^{-1} by setting a step time of 10 h of discharge and charge. We may estimate for this cell a practical energy exceeding 450 W h kg^{-1} which is a value well competing and exceeding the one ascribed to the common Li-ion battery.[1] Furthermore, the cell can deliver a satisfactory value of the capacity referred to geometric electrode surface area (*i.e.*, of about 1 mA h cm^{-2}) which may be further improved by changing the loading of the SPC, or by replacing the substrate at the cathode side with more efficient media such as those including catalysts or nanostructures for fastening the electrochemical process, increasing the capacity, further limiting the ORR/OER polarization, and finally achieving Li/O_2 batteries of long life and practical interest.

CONCLUSIONS

New configurations of glyme-based electrolytes have been investigated in this work for improving the performances of the lithium−oxygen battery. Various electrolytes were reported in the literature for a Li/O_2 cell such as a triglyme dissolving LiTFSI[69] and *N*,*N*-dimethylacetamide dissolving $LiNO_3$ with different concentrations,[37] while a triglyme with $LiCF_3SO_3$ and $LiNO_3$ was proposed for the Li/$LiFePO_4$ cell.[25] Herein, we originally dissolved relevant concentrations of the conducting salt (LiTFSI) and the sacrificial agent ($LiNO_3$) and studied the correlation between the characteristics of the SEI layer, the solvent volatility, and the Li/O_2 cycling performance. Indeed, almost saturated solutions were employed to increase the safety and limit the electrolyte evaporation, as well as to consolidate the SEI layer at the lithium surface and achieve efficient protection of the reactive metal anode. Despite artificial SEI possibly allowing Li/O_2 cell operation, our approach has foreseen *in situ* formation of the layer without employing additional chemicals or physical agents, thus advantageously lowering the cell impact. The outer/inner composition of the complex SEI on lithium samples was therefore analyzed by XPS measurements upon Ar^+ etching. The measurement revealed the mainly inorganic nature of the inner layer of the SEI formed by fast reactions on the metal to form LiF, Li_2CO_3, LiN_xO_y, and Li_2O and the organic character of the outer SEI accounting for minor electrolytes reduction to ROLi and ROR species with side precipitation of LiTFSI. These features hindered further deterioration of DEGDME_HCE and TREGDME_HCE at the lithium surface and suggested possible application of the electrolytes in an efficient and stable battery. Subsequently, TGA depicted a thermal stability of DEGDME_HCE extended up to 80 °C and a higher value for TREGDME_HCE, that is, above 130 °C, because of a more relevant salt concentration and longer glyme chain of the latter compared to the former, thus suggesting TREGDME_HCE as a more suitable candidate for application in an open environment. Further weight losses were observed between 200 and 400 °C and above 400 °C, ascribed to the removal of the glyme from crystallized salt−solvent complexes

https://dx.doi.org/10.1021/acsaem.0c02331
ACS Appl. Energy Mater. 2020, 3, 12263−12275

throughout a multistep dry-recrystallization mechanism and to LiTFSI salt degradation, respectively. On the other hand, the electrochemical investigation revealed for DEGDME_HCE an ionic conductivity ranging from 3×10^{-3} to 8×10^{-3} S cm^{-1}, a Li^+ transference number of about 0.60, and a stability window extending from about 0 up to 4.3 V *versus* Li^+/Li, whereas TREGDME_HCE has shown lower conductivity (from 9×10^{-4} to 2×10^{-3} S cm^{-1}) and Li^+ transference number (about 0.5), while a higher anodic stability with an oxidation potential of 4.4 V *versus* Li^+/Li. Both electrolytes revealed a limited lithium/electrolyte interphase resistance and the absence of dendritic structure formation upon prolonged galvanostatic cycling, thus confirming the consolidation of a stable SEI on the metal surface. The applicability in lithium−oxygen cells of the electrolytes was investigated by means of EIS measurements upon cell aging in a pure O_2 atmosphere. The cell using DEGDME_HCE revealed a rapid increase of the resistance from 83 Ω to about 3900 Ω after 8 days of storage because of progressive degradation of the electrode/electrolyte interphase and possibly DEGDME solvent volatilization leading to the formation of a grain boundary. Instead, the cell using TREGDME_HCE has shown a very stable resistance trend with a final value of about 270 Ω after 28 days of measurement and only limited modifications because of the consolidation of the SEI. Indeed, DEGDME_HCE provided the reversible discharge/charge process only for few cycles, which was hindered by significant increase in polarization, while TREGDME_HCE stably delivered a reversible capacity of 500 mA h g^{-1}, in particular after an aging process designed in order to allow the consolidation of the SEI layer. We have estimated for the above cell a theoretical energy density of 1350 W h kg^{-1} and a practical value of 270 W h kg^{-1}, which is comparable to the one delivered by lithium-ion batteries. Furthermore, a preliminary test at 1000 mA h g^{-1} indicated a possible increase in the practical energy density value above 450 W h kg^{-1}. Therefore, our study indicated intrinsic properties of the concentrated electrolytes and suggested TREGDME_HCE for the Li/O_2 battery.

■ ASSOCIATED CONTENT

Supporting Information

The Supporting Information is available free of charge at https://pubs.acs.org/doi/10.1021/acsaem.0c02331.

X-ray photoelectron survey spectra recorded at various Ar^+ sputtering times carried out on the surfaces of lithium foils soaked with the electrolytes; Nyquist plots recorded at various temperatures by EIS on stainless-steel symmetrical cells to determine the ionic conductivity; chronoamperometric curves and Nyquist plots recorded by EIS before and after polarization used to determine the Li^+ transference number in Li/Li symmetrical cells by employing the Bruce−Vincent−Evans equation; Properties of various glymes with different chain length; Nyquist plots and corresponding interphase resistance trends recorded by EIS upon aging for 14 h and prolonged aging for 23 days of symmetrical Li/Li cells using the electrolytes and NLLS analyses carried out through a Boukamp tool on the Nyquist plots; NLLS analyses of the Nyquist plots recorded by EIS upon aging of lithium−oxygen cells; Weight % trends of electrolyte samples upon prolonged exposure to ambient conditions at the room temperature (25 °C); and voltage profiles of a lithium−oxygen cell exploiting the Li/TREGDME_HCE/SPC-O_2 configuration galvanostatically cycled with specific capacity limited to 1000 mA h g^{-1} referred to the SPC mass (PDF)

■ AUTHOR INFORMATION

Corresponding Authors

Julian Morales − *Dpto. Química Inorgánica e Ingeniería Química, Instituto de Química Fina y Nanoquímica, Universidad de Córdoba, 14071 Córdoba, Spain;* orcid.org/0000-0001-5455-1682; Email: iq1mopaj@uco.es

Jusef Hassoun − *Department of Chemical and Pharmaceutical Sciences and National Interuniversity Consortium of Materials Science and Technology (INSTM) University of Ferrara Research Unit, University of Ferrara, 44121 Ferrara, Italy;* orcid.org/0000-0002-8218-5680; Email: jusef.hassoun@unife.it

Authors

Vittorio Marangon − *Department of Chemical and Pharmaceutical Sciences, University of Ferrara, 44121 Ferrara, Italy;* orcid.org/0000-0003-4722-8988

Celia Hernandez-Rentero − *Dpto. Química Inorgánica e Ingeniería Química, Instituto de Química Fina y Nanoquímica, Universidad de Córdoba, 14071 Córdoba, Spain*

Stanislav Levchenko − *Department of Chemical and Pharmaceutical Sciences, University of Ferrara, 44121 Ferrara, Italy*

Giacomo Bianchini − *Department of Chemical and Pharmaceutical Sciences, University of Ferrara, 44121 Ferrara, Italy*

Davide Spagnolo − *Department of Chemical and Pharmaceutical Sciences, University of Ferrara, 44121 Ferrara, Italy*

Alvaro Caballero − *Dpto. Química Inorgánica e Ingeniería Química, Instituto de Química Fina y Nanoquímica, Universidad de Córdoba, 14071 Córdoba, Spain;* orcid.org/0000-0002-2084-0686

Complete contact information is available at: https://pubs.acs.org/10.1021/acsaem.0c02331

Notes

The authors declare no competing financial interest.

■ ACKNOWLEDGMENTS

The authors thank the University of Ferrara for funding (Fondo di Ateneo per la Ricerca Locale, FAR 2019) and the agreement "Accordo di Collaborazione Quadro 2015" between University of Ferrara (Department of Chemical and Pharmaceutical Sciences) and Sapienza University of Rome (Department of Chemistry). The research was also funded by Ministerio de Economía y Competitividad (Project MAT2017-87541-R) and Junta de Andalucía (Group FQM-175).

■ REFERENCES

(1) Di Lecce, D.; Verrelli, R.; Hassoun, J. Lithium-Ion Batteries for Sustainable Energy Storage: Recent Advances towards New Cell Configurations. *Green Chem.* **2017**, *19*, 3442−3467.

(2) Van Noorden, R. The Rechargeable Revolution: A Better Battery. *Nature* **2014**, *507*, 26−28.

(3) Abraham, K. M. Prospects and Limits of Energy Storage in Batteries. *J. Phys. Chem. Lett.* **2015**, *6*, 830−844.
(4) Lu, L.; Han, X.; Li, J.; Hua, J.; Ouyang, M. A Review on the Key Issues for Lithium-Ion Battery Management in Electric Vehicles. *J. Power Sources* **2013**, *226*, 272−288.
(5) Yoo, H. D.; Markevich, E.; Salitra, G.; Sharon, D.; Aurbach, D. On the Challenge of Developing Advanced Technologies for Electrochemical Energy Storage and Conversion. *Mater. Today* **2014**, *17*, 110−121.
(6) Choudhury, S.; Mangal, R.; Agrawal, A.; Archer, L. A. A Highly Reversible Room-Temperature Lithium Metal Battery Based on Crosslinked Hairy Nanoparticles. *Nat. Commun.* **2015**, *6*, 10101.
(7) Xu, W.; Wang, J.; Ding, F.; Chen, X.; Nasybulin, E.; Zhang, Y.; Zhang, J.-G. Lithium Metal Anodes for Rechargeable Batteries. *Energy Environ. Sci.* **2014**, *7*, 513−537.
(8) Erickson, E. M.; Ghanty, C.; Aurbach, D. New Horizons for Conventional Lithium Ion Battery Technology. *J. Phys. Chem. Lett.* **2014**, *5*, 3313−3324.
(9) Hassoun, J.; Croce, F.; Armand, M.; Scrosati, B. Investigation of the O_2 Electrochemistry in a Polymer Electrolyte Solid-State Cell. *Angew. Chem., Int. Ed.* **2011**, *50*, 2999−3002.
(10) Carbone, L.; Greenbaum, S. G.; Hassoun, J. Lithium Sulfur and Lithium Oxygen Batteries: New Frontiers of Sustainable Energy Storage. *Sustain. Energy Fuels* **2017**, *1*, 228−247.
(11) Wang, Q.; Ping, P.; Zhao, X.; Chu, G.; Sun, J.; Chen, C. Thermal Runaway Caused Fire and Explosion of Lithium Ion Battery. *J. Power Sources* **2012**, *208*, 210−224.
(12) Lin, D.; Liu, Y.; Cui, Y. Reviving the Lithium Metal Anode for High-Energy Batteries. *Nat. Nanotechnol.* **2017**, *12*, 194−206.
(13) Freunberger, S. A.; Chen, Y.; Peng, Z.; Griffin, J. M.; Hardwick, L. J.; Bardé, F.; Novák, P.; Bruce, P. G. Reactions in the Rechargeable Lithium-O_2 Battery with Alkyl Carbonate Electrolytes. *J. Am. Chem. Soc.* **2011**, *133*, 8040−8047.
(14) Jung, H.-G.; Hassoun, J.; Park, J.-B.; Sun, Y.-K.; Scrosati, B. An Improved High-Performance Lithium−Air Battery. *Nat. Chem.* **2012**, *4*, 579−585.
(15) Elia, G. A.; Bresser, D.; Reiter, J.; Oberhumer, P.; Sun, Y.-K.; Scrosati, B.; Passerini, S.; Hassoun, J. Interphase Evolution of a Lithium-Ion/Oxygen Battery. *ACS Appl. Mater. Interfaces* **2015**, *7*, 22638−22643.
(16) Di Lecce, D.; Fasciani, C.; Scrosati, B.; Hassoun, J. A Gel−Polymer Sn−C/$LiMn_{0.5}Fe_{0.5}PO_4$ Battery Using a Fluorine-Free Salt. *ACS Appl. Mater. Interfaces* **2015**, *7*, 21198−21207.
(17) Appetecchi, G. B.; Croce, F.; Hassoun, J.; Scrosati, B.; Salomon, M.; Cassel, F. Hot-Pressed, Dry, Composite, PEO-Based Electrolyte Membranes. *J. Power Sources* **2003**, *114*, 105−112.
(18) Kimura, K.; Matsumoto, H.; Hassoun, J.; Panero, S.; Scrosati, B.; Tominaga, Y. A QuaternaryPoly(Ethylene Carbonate)-Lithium Bis(Trifluoromethanesulfonyl)Imide-Ionic Liquid-Silica Fiber Composite Polymer Electrolyte for Lithium Batteries. *Electrochim. Acta* **2015**, *175*, 134−140.
(19) Yamada, T.; Ito, S.; Omoda, R.; Watanabe, T.; Aihara, Y.; Agostini, M.; Ulissi, U.; Hassoun, J.; Scrosati, B. All Solid-State Lithium-Sulfur Battery Using a Glass-Type P_2S_5-Li_2S Electrolyte: Benefits on Anode Kinetics. *J. Electrochem. Soc.* **2015**, *162*, A646−A651.
(20) Di Lecce, D.; Minnetti, L.; Polidoro, D.; Marangon, V.; Hassoun, J. Triglyme-Based Electrolyte for Sodium-Ion and Sodium-Sulfur Batteries. *Ionics* **2019**, *25*, 3129−3141.
(21) Tobishima, S.; Morimoto, H.; Aoki, M.; Saito, Y.; Inose, T.; Fukumoto, T.; Kuryu, T. Glyme-Based Nonaqueous Electrolytes for Rechargeable Lithium Cells. *Electrochim. Acta* **2004**, *49*, 979−987.
(22) Aurbach, D.; Granot, E. The Study of Electrolyte Solutions Based on Solvents from the "Glyme" Family (Linear Polyethers) for Secondary Li Battery Systems. *Electrochim. Acta* **1997**, *42*, 697−718.
(23) Carbone, L.; Gobet, M.; Peng, J.; Devany, M.; Scrosati, B.; Greenbaum, S.; Hassoun, J. Comparative Study of Ether-Based Electrolytes for Application in Lithium−Sulfur Battery. *ACS Appl. Mater. Interfaces* **2015**, *7*, 13859−13865.
(24) Di Lecce, D.; Carbone, L.; Gancitano, V.; Hassoun, J. Rechargeable Lithium Battery Using Non-Flammable Electrolyte Based on Tetraethylene Glycol Dimethyl Ether and Olivine Cathodes. *J. Power Sources* **2016**, *334*, 146−153.
(25) Carbone, L.; Di Lecce, D.; Gobet, M.; Munoz, S.; Devany, M.; Greenbaum, S.; Hassoun, J. Relevant Features of a Triethylene Glycol Dimethyl Ether-Based Electrolyte for Application in Lithium Battery. *ACS Appl. Mater. Interfaces* **2017**, *9*, 17085−17095.
(26) Carbone, L.; Moro, P. T.; Gobet, M.; Munoz, S.; Devany, M.; Greenbaum, S. G.; Hassoun, J. Enhanced Lithium Oxygen Battery Using a Glyme Electrolyte and Carbon Nanotubes. *ACS Appl. Mater. Interfaces* **2018**, *10*, 16367−16375.
(27) Xu, W.; Xu, K.; Viswanathan, V. V.; Towne, S. A.; Hardy, J. S.; Xiao, J.; Nie, Z.; Hu, D.; Wang, D.; Zhang, J.-G. Reaction Mechanisms for the Limited Reversibility of Li-O_2 Chemistry in Organic Carbonate Electrolytes. *J. Power Sources* **2011**, *196*, 9631−9639.
(28) Ming, J.; Cao, Z.; Wu, Y.; Wahyudi, W.; Wang, W.; Guo, X.; Cavallo, L.; Hwang, J.-Y.; Shamim, A.; Li, L.-J.; Sun, Y.-K.; Alshareef, H. N. New Insight on the Role of Electrolyte Additives in Rechargeable Lithium Ion Batteries. *ACS Energy Lett.* **2019**, *4*, 2613−2622.
(29) Xiong, S.; Xie, K.; Diao, Y.; Hong, X. Properties of Surface Film on Lithium Anode with $LiNO_3$ as Lithium Salt in Electrolyte Solution for Lithium−sulfur Batteries. *Electrochim. Acta* **2012**, *83*, 78−86.
(30) Lee, S. H.; Hwang, J. Y.; Ming, J.; Cao, Z.; Nguyen, H. A.; Jung, H. G.; Kim, J.; Sun, Y. K. Toward the Sustainable Lithium Metal Batteries with a New Electrolyte Solvation Chemistry. *Adv. Energy Mater.* **2020**, *10*, 2000567.
(31) Winter, M. The Solid Electrolyte Interphase − The Most Important and the Least Understood Solid Electrolyte in Rechargeable Li Batteries. *Z. Phys. Chem.* **2009**, *223*, 1395−1406.
(32) Aurbach, D. Review of Selected Electrode−solution Interactions Which Determine the Performance of Li and Li Ion Batteries. *J. Power Sources* **2000**, *89*, 206−218.
(33) Zhang, S. S. Role of $LiNO_3$ in Rechargeable Lithium/Sulfur Battery. *Electrochim. Acta* **2012**, *70*, 344−348.
(34) Rosenman, A.; Elazari, R.; Salitra, G.; Markevich, E.; Aurbach, D.; Garsuch, A. The Effect of Interactions and Reduction Products of $LiNO_3$, the Anti-Shuttle Agent, in Li-S Battery Systems. *J. Electrochem. Soc.* **2015**, *162*, A470−A473.
(35) Zhang, S.; Ueno, K.; Dokko, K.; Watanabe, M. Recent Advances in Electrolytes for Lithium-Sulfur Batteries. *Adv. Energy Mater.* **2015**, *5*, 1500117.
(36) Lee, D.-J.; Agostini, M.; Park, J.-W.; Sun, Y.-K.; Hassoun, J.; Scrosati, B. Progress in Lithium-Sulfur Batteries: The Effective Role of a Polysulfide-Added Electrolyte as Buffer to Prevent Cathode Dissolution. *ChemSusChem* **2013**, *6*, 2245−2248.
(37) Yoo, E.; Qiao, Y.; Zhou, H. Understanding the Effect of the Concentration of $LiNO_3$ Salt in Li-O_2 Batteries. *J. Mater. Chem. A* **2019**, *7*, 18318−18323.
(38) Sharon, D.; Hirsberg, D.; Afri, M.; Chesneau, F.; Lavi, R.; Frimer, A. a.; Sun, Y.-K.; Aurbach, D. Catalytic Behavior of Lithium Nitrate in Li-O_2 Cells. *ACS Appl. Mater. Interfaces* **2015**, *7*, 16590−16600.
(39) Giordani, V.; Tozier, D.; Tan, H.; Burke, C. M.; Gallant, B. M.; Uddin, J.; Greer, J. R.; McCloskey, B. D.; Chase, G. V.; Addison, D. A Molten Salt Lithium-Oxygen Battery. *J. Am. Chem. Soc.* **2016**, *138*, 2656−2663.
(40) Suo, L.; Hu, Y.-S.; Li, H.; Armand, M.; Chen, L. A New Class of Solvent-in-Salt Electrolyte for High-Energy Rechargeable Metallic Lithium Batteries. *Nat. Commun.* **2013**, *4*, 1481.
(41) Ruggeri, I.; La Monaca, A.; De Giorgio, F.; Soavi, F.; Arbizzani, C.; Berbenni, V.; Ferrara, C.; Mustarelli, P. Correlating Structure and Properties of Super-Concentrated Electrolyte Solutions: ^{17}O NMR and Electrochemical Characterization. *ChemElectroChem* **2019**, *6*, 4002−4009.
(42) Liu, B.; Xu, W.; Yan, P.; Sun, X.; Bowden, M. E.; Read, J.; Qian, J.; Mei, D.; Wang, C.-M.; Zhang, J.-G. Enhanced Cycling Stability of

Rechargeable Li-O_2 Batteries Using High-Concentration Electrolytes. *Adv. Funct. Mater.* **2016**, *26*, 605−613.
(43) Camacho-Forero, L. E.; Smith, T. W.; Balbuena, P. B. Effects of High and Low Salt Concentration in Electrolytes at Lithium-Metal Anode Surfaces. *J. Phys. Chem. C* **2017**, *121*, 182−194.
(44) Evans, J.; Vincent, C. A.; Bruce, P. G. Electrochemical Measurement of Transference Numbers in Polymer Electrolytes. *Polymer* **1987**, *28*, 2324−2328.
(45) Boukamp, B. Nonlinear Least Squares Fit Procedure for Analysis of Immittance Data of Electrochemical Systems. *Solid State Ionics* **1986**, *20*, 31−44.
(46) Boukamp, B. A Package for Impedance/Admittance Data Analysis. *Solid State Ionics* **1986**, *18*−*19*, 136−140.
(47) Liu, Q.; Cresce, A.; Schroeder, M.; Xu, K.; Mu, D.; Wu, B.; Shi, L.; Wu, F. Insight on Lithium Metal Anode Interphasial Chemistry: Reduction Mechanism of Cyclic Ether Solvent and SEI Film Formation. *Energy Storage Mater.* **2019**, *17*, 366−373.
(48) Dedryvère, R.; Leroy, S.; Martinez, H.; Blanchard, F.; Lemordant, D.; Gonbeau, D. XPS Valence Characterization of Lithium Salts as a Tool to Study Electrode/Electrolyte Interfaces of Li-Ion Batteries. *J. Phys. Chem. B* **2006**, *110*, 12986−12992.
(49) Di Lecce, D.; Marangon, V.; Benítez, A.; Caballero, Á.; Morales, J.; Rodríguez-Castellón, E.; Hassoun, J. High Capacity Semi-Liquid Lithium Sulfur Cells with Enhanced Reversibility for Application in New-Generation Energy Storage Systems. *J. Power Sources* **2019**, *412*, 575−585.
(50) Kanamura, K.; Tamura, H.; Shiraishi, S.; Takehara, Z.-I. XPS Analysis for the Lithium Surface Immersed in γ-Butyrolactone Containing Various Salts. *Electrochim. Acta* **1995**, *40*, 913−921.
(51) Vargas, Ó.; Caballero, Á.; Morales, J.; Rodríguez-Castellón, E. Contribution to the Understanding of Capacity Fading in Graphene Nanosheets Acting as an Anode in Full Li-Ion Batteries. *ACS Appl. Mater. Interfaces* **2014**, *6*, 3290−3298.
(52) Veith, G. M.; Nanda, J.; Delmau, L. H.; Dudney, N. J. Influence of Lithium Salts on the Discharge Chemistry of Li-Air Cells. *J. Phys. Chem. Lett.* **2012**, *3*, 1242−1247.
(53) Ensling, D.; Stjerndahl, M.; Nytén, A.; Gustafsson, T.; Thomas, J. O. A Comparative XPS Surface Study of Li_2FeSiO_4/C Cycled with LiTFSI- and $LiPF_6$-Based Electrolytes. *J. Mater. Chem.* **2009**, *19*, 82−88.
(54) Agostini, M.; Xiong, S.; Matic, A.; Hassoun, J. Polysulfide-Containing Glyme-Based Electrolytes for Lithium Sulfur Battery. *Chem. Mater.* **2015**, *27*, 4604−4611.
(55) Tułodziecki, M.; Tarascon, J.-M.; Taberna, P.-L.; Guéry, C. Catalytic Reduction of TFSI-Containing Ionic Liquid in the Presence of Lithium Cations. *Electrochem. Commun.* **2017**, *77*, 128−132.
(56) Aurbach, D.; Weissman, I.; Schechter, A.; Cohen, H. X-Ray Photoelectron Spectroscopy Studies of Lithium Surfaces Prepared in Several Important Electrolyte Solutions. A Comparison with Previous Studies by Fourier Transform Infrared Spectroscopy. *Langmuir* **1996**, *12*, 3991−4007.
(57) Schechter, A.; Aurbach, D.; Cohen, H. X-Ray Photoelectron Spectroscopy Study of Surface Films Formed on Li Electrodes Freshly Prepared in Alkyl Carbonate Solutions. *Langmuir* **1999**, *15*, 3334−3342.
(58) Yao, K. P. C.; Kwabi, D. G.; Quinlan, R. A.; Mansour, A. N.; Grimaud, A.; Lee, Y.-L.; Lu, Y.-C.; Shao-Horn, Y. Thermal Stability of Li_2O_2 and Li_2O for Li-Air Batteries: In Situ XRD and XPS Studies. *J. Electrochem. Soc.* **2013**, *160*, A824−A831.
(59) Elia, G. A.; Bernhard, R.; Hassoun, J. A Lithium-Ion Oxygen Battery Using a Polyethylene Glyme Electrolyte Mixed with an Ionic Liquid. *RSC Adv.* **2015**, *5*, 21360−21365.
(60) Carbone, L.; Gobet, M.; Peng, J.; Devany, M.; Scrosati, B.; Greenbaum, S.; Hassoun, J. Comparative Study of Ether-Based Electrolytes for Application in Lithium-Sulfur Battery. *ACS Appl. Mater. Interfaces* **2015**, *7*, 13859−13865.
(61) Shimizu, K.; Freitas, A. A.; Atkin, R.; Warr, G. G.; FitzGerald, P. A.; Doi, H.; Saito, S.; Ueno, K.; Umebayashi, Y.; Watanabe, M.; Canongia Lopes, J. N. Structural and Aggregate Analyses of (Li Salt + Glyme) Mixtures: The Complex Nature of Solvate Ionic Liquids. *Phys. Chem. Chem. Phys.* **2015**, *17*, 22321−22335.
(62) Ueno, K.; Yoshida, K.; Tsuchiya, M.; Tachikawa, N.; Dokko, K.; Watanabe, M. Glyme-Lithium Salt Equimolar Molten Mixtures: Concentrated Solutions or Solvate Ionic Liquids? *J. Phys. Chem. B* **2012**, *116*, 11323−11331.
(63) Marangon, V.; Tominaga, Y.; Hassoun, J. An Alternative Composite Polymer Electrolyte for High Performances Lithium Battery. *J. Power Sources* **2020**, *449*, 227508.
(64) Wei, S.; Li, Z.; Kimura, K.; Inoue, S.; Pandini, L.; Di Lecce, D.; Tominaga, Y.; Hassoun, J. Glyme-Based Electrolytes for Lithium Metal Batteries Using Insertion Electrodes: An Electrochemical Study. *Electrochim. Acta* **2019**, *306*, 85−95.
(65) Goodenough, J. B.; Kim, Y. Challenges for Rechargeable Li Batteries. *Chem. Mater.* **2010**, *22*, 587−603.
(66) Hernández-Rentero, C.; Marangon, V.; Olivares-Marín, M.; Gómez-Serrano, V.; Caballero, Á.; Morales, J.; Hassoun, J. Alternative Lithium-Ion Battery Using Biomass-Derived Carbons as Environmentally Sustainable Anode. *J. Colloid Interface Sci.* **2020**, *573*, 396−408.
(67) Kim, G.-T.; Appetecchi, G. B.; Alessandrini, F.; Passerini, S. Solvent-Free, PYR_{1A}TFSI Ionic Liquid-Based Ternary Polymer Electrolyte Systems. I. Electrochemical Characterization. *J. Power Sources* **2007**, *171*, 861−869.
(68) Lau, S.; Archer, L. A. Nucleation and Growth of Lithium Peroxide in the Li−O_2 Battery. *Nano Lett.* **2015**, *15*, 5995−6002.
(69) Kwon, H.-M.; Thomas, M. L.; Tatara, R.; Oda, Y.; Kobayashi, Y.; Nakanishi, A.; Ueno, K.; Dokko, K.; Watanabe, M. Stability of Glyme Solvate Ionic Liquid as an Electrolyte for Rechargeable Li−O_2 Batteries. *ACS Appl. Mater. Interfaces* **2017**, *9*, 6014−6021.

https://dx.doi.org/10.1021/acsaem.0c02331
ACS Appl. Energy Mater. 2020, 3, 12263−12275